



Controlled drug release of parylene-coated pramipexole nanofibers for transdermal applications

Serdar Tort^{a,b}, Daewoo Han^a, Eric Frantz^a, Andrew J. Steckl^{a,*}

^a Nanoelectronics Laboratory, Electrical Engineering and Computer Science, University of Cincinnati, Cincinnati 45221-0030, USA

^b Department of Pharmaceutical Technology, Faculty of Pharmacy, Gazi University, Ankara 06330, Turkey

ARTICLE INFO

Keywords:

Electrospinning
Chemical vapor deposition process
Parylene
Controlled drug release
Transdermal nanofibers
Pramipexole

ABSTRACT

Electrospun nanofibers are promising drug delivery systems for transdermal applications with a release rate of the drug depending on the host polymer used. However, it is still a challenge to control (*i.e.*, reduce) the release rate for hydrophilic drugs in order to provide long-term sustained release. In this study, we aimed to produce controlled release nanofibers to achieve long term drug release for transdermal applications. Pramipexole, which requires multiple doses per day, was selected as a hydrophilic model drug molecule and was electrospun with hydrophobic polycaprolactone polymer. To prevent burst release of the drug and provide a long-term release profile, nanofibers were coated with Parylene C or N using a chemical vapor deposition process. The effective thickness of nanofibers increased with the amount of Parylene coating. Parylene coating also enhanced the mechanical properties and hydrophobicity but decreased the bioadhesion values. Drug release and diffusion studies showed that Parylene coating successfully prevents drug burst release. Uncoated nanofibers completely released pramipexole within 12 h. A relatively low amount of Parylene N and C coating provided 81% and 52% drug release over 10 days, while increased Parylene N and C coating resulted in 27% and 12.6% drug release over a 30-day period, respectively. Parylene coating process offers the possibility of long-term controlled release kinetics including hydrophilic drugs.

1. Introduction

Transdermal drug delivery can be used for either local or systemic therapy and has some advantages compared to other drug delivery routes, such as ease of use, non-invasiveness and avoiding the first-pass effect of the hepatic metabolism and enzymatic degradation by the gastrointestinal tract. In particular, for elderly individuals who are under chronic therapy and unable to take oral medications, transdermal methods are good candidates for drug applications. Drug release kinetics from transdermal drug delivery systems are designed by considering a polymer matrix, membrane and drug properties. Other excipients, such as permeation enhancers or plasticizers, can also be considered in the formulations. Transdermal drug delivery systems have been prepared by various methods, including solvent casting, aluminum backed adhesive film, mercury substrate, and fiber electrospinning [1–4].

Electrospinning is a very attractive fiber production method and has opened a new era for nano-scaled pharmaceutical applications with superior mechanical and functional properties of nanofibers [5,6]. Membranes formed from electrospun nanofibers have large surface area,

high porosity and ability to control the drug release rate [7,8]. In addition, nanofiber membranes are flexible and robust for site specific applications, such as face masks [9] and wound dressings [6]. In terms of transdermal applications, transdermal nanofiber patches have more flexible characteristics than transdermal patches prepared by solvent casting method [10].

Pramipexole (PPX) is a good candidate for transdermal drug delivery because it is very effective even at low concentration in plasma [11]. Various PPX formulations are currently marketed with immediate release or extended release dosage properties. Extended release dosage forms provide a constant drug concentration in plasma and prevent recurrence of symptoms, such as tremor and bradykinesia incurred by drug elimination. However, there are limited studies on transdermal PPX delivery to date. Li et al. prepared PPX nanocrystals for transdermal delivery using a wet milling method. PPX nanocrystals containing carbomer gel provided higher permeation profile than coarse suspension gel, improving transdermal delivery of the drug [12]. In another study, Wang et al. prepared PPX-containing transdermal patches using solution casting onto the fluoride-coated polyester release liner, which provide a

* Corresponding author.

E-mail address: a.steckl@uc.edu (A.J. Steckl).

sustained drug release for one week. They found that the long-term delivery of PPX improves the symptoms and prevent the neurodegenerative processes by inhibiting oxidative stress and mitochondrial apoptosis pathway [11].

Poly(para-xylylene), also known as Parylene, forms a protective barrier film when applied to substrate surfaces. They are classified as thermoplastic polymers and a thin layer can be formed on substrate surfaces by chemical vapor deposition (CVD) followed by polymerization. There are six types of Parylene: N, C, D, HT, AF-4 and F. Each Parylene type has different chemical, electrical and physical properties (Table 1). Parylene N is the basic member of the poly-p-xylylene series, assuming the form of a completely linear, highly crystalline material with the repeating unit consisting of a carbon-hydrogen combination. Parylene C, the most widely used Parylene for conformal coatings, is a poly-monochloro para-xylylene, produced from the same dimer material with Parylene N, with one chlorine group on its main-chain phenyl ring. In biomedical applications, Parylene C is frequently used due to its dense structure with smooth hydrophobic surface [13]. Parylene coating reduces surface wettability due to its hydrophobic nature, which provides the beneficial effect of corrosion resistance of implantable and biodegradable magnesium alloys. It also offers numerous advantages over conventional polymeric materials, such as low water permeability, durability, and biocompatibility.

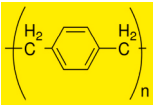
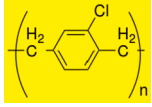
Parylene coating can provide controlled release of encapsulated materials by acting as a barrier in drug delivery systems, which has been used in conjunction with doxorubicin, dexamethasone and amiodarone for providing sustained drug release [14–16]. Parylene has also been used to coat drug eluting stents [17]. Only a few reports have been published regarding Parylene coated nanofibers, for example on the use of Parylene C for coating cellulose nanofibers to provide improved oxygen barrier and water resistance in food packaging [18]. In our studies, two types of Parylenes (C and N) were used in coating studies of PPX-loaded PCL nanofiber patches for controlled transdermal drug delivery. In addition, the impact of the amount of Parylene used in the coating process was also evaluated on drug release kinetics. Detailed material characterization studies, such as XRD, DSC, and NMR, on nanofibers were performed. The effect of Parylene coating on the mechanical, bioadhesion and wettability properties of nanofibers was investigated.

2. Materials and methods

2.1. Materials

Parylene C and N dimers were obtained from Specialty Coating Systems (Indianapolis, IN). Polycaprolactone (PCL, Mw 80 kDa) and cellulose membranes for dialysis (with 12 kDa cut off) were purchased from MilliporeSigma (Burlington, MA). PPX drug, glacial acetic acid, and formic acid solvents were purchased from Fisher Scientific (Waltham, MA).

Table 1
Specifications and properties of Parylene N and C [38].

Properties	Parylene N	Parylene C
Chemical formula		
Dielectric constant (60 Hz)	2.65	3.15
Moisture vapor transmission rate (g · mm)/(m ² · day)	0.59	0.08
Melting point (°C)	420	290
Tensile strength (MPa)	51.72	68.97
Elongation at break (%)	Up to 250	Up to 200
Oxygen permeability (cc · mm)/(m ² · day · atm)	15.4	2.8

2.2. Electrospinning solutions

Different formulations were used for investigating the nanofiber based transdermal drug delivery system, as shown in Table 2. All electrospinning solutions were prepared in glacial acetic acid (GAA) and formic acid (FA) mixture with a 3:1 volume ratio. For this purpose, accurately weighted PPX was dissolved in FA, then GAA was added to this solution. PCL was added to PPX containing GAA-FA mixture and stirred until a clear solution is obtained at room temperature. Before the electrospinning process, rheological properties of PCL solutions without and with PPX were investigated to evaluate the effect of PPX in solution. For this purpose, a cone-plate viscosimeter (Brookfield rheometer DV-3DV) was used at different shear rates with spindle number 52. Prepared solutions were electrospun with the following conditions: 17 kV applied voltage, 0.3 mL/h flow rate and needle-to-collector distance of 17 cm.

2.3. Coating of PCL nanofibers

PPX-loaded PCL nanofibers were coated with Parylene using CVD. CVD provides a pinhole-free uniform coating of Parylene [17] whereas alternative methods (e.g. dip coating, spray deposition) have some disadvantages, such as air bubbles, bridging and sloughing. The CVD thin film deposition of Parylene consists of three steps: sublimation, pyrolysis and polymerization. Briefly, solid granular Parylene (“dimer”) is heated ($T > 100$ °C) to produce dimeric gas, which is then pyrolyzed to form gaseous monomers ($T > 500$ °C) that are adsorbed on surfaces. In the final step, polymerization of the monomers forming a conformal film on the target surface. In our studies, two types of Parylene (C and N) were used with two different granular amounts (50 and 300 mg) using a Parylene-specific CVD system (Specialty Coating Systems PDS 2010).

2.4. SEM observations

Detailed images of nanofiber membranes were obtained with SEM (Quanta 400F Field Emission SEM) at an acceleration voltage of 20 kV to observe the morphology of nanofibers. All samples were sputter-coated with gold/palladium to make them conductive for preventing sample charging effect during SEM observation. The mean fiber diameter was measured from 50 different nanofibers for each sample by using ImageJ software (National Institutes of Health, USA).

2.5. DSC studies

Differential scanning calorimetry (DSC) thermograms were obtained to observe possible interactions between drug, host polymer and Parylene coatings. Accurately weighed (~2 mg) samples of PPX, PCL, Parylene or nanofiber membranes were placed in an aluminum pan and sealed immediately. DSC measurements were performed under nitrogen atmosphere at a heating rate of 10 °C/min.

2.6. NMR and XRD studies

NMR and XRD studies provide information about the chemical changes and molecular structure of materials after the electrospinning

Table 2
Composition of different electrospinning solutions and membrane coating materials.

Formulation code	PPX (%)	PCL (%)	Parylene C (mg)	Parylene N (mg)
PCL	0.5	10	–	–
PPC50	0.5	10	50	–
PPN50	0.5	10	–	50
PPC300	0.5	10	300	–
PPN300	0.5	10	–	300

process. ^1H NMR spectra were recorded on a Varian Mercury 400 MHz High Performance Digital FT-NMR spectrometer (Agilent Technologies, Santa Clara, CA, USA) using tetramethyl silane as the internal standard and DMSO as solvent. Chemical shifts are given in δ (ppm). All coupling constants are reported as Hertz. XRD analyses were performed on a Rigaku Miniflex X-Ray diffractometer (Rigaku Corporation, Tokyo, Japan) using Cu $K\alpha$ radiation, 30 kV voltage, 15 mA current in 2θ ranges of $3\text{--}40^\circ$.

2.7. Wettability and porosity of nanofibers

To characterize the surface wettability of nanofiber membranes, water contact angles (WCA) on nanofiber membranes were measured with an optical tensiometer (First Ten Angstroms, 1000 B Drop Shape Instrument). 5 μL distilled water droplets were placed on different nanofiber membranes and the contact angle between the surface and the water droplet was measured. For comparison, PCL films were prepared by solvent casting method. PCL pellets were dissolved in chloroform and placed in a Petri dish. Petri dishes were placed overnight in a fume hood to evaporate the solvent. An average WCA was calculated from three measurements. The porosities of nanofiber membranes before and after Parylene coating were calculated based on the following equations without and with PPXs [19]. For this purpose, the following equations were used:

$$\text{membrane apparent density} = \text{mass}/(\text{area} \times \text{thickness}) \quad (1)$$

$$\text{membrane porosity} = 1 - (\text{membrane apparent density}/\text{bulk density}) \quad (2)$$

2.8. Mechanical properties

Mechanical tensile strength and elongation at break values of coated and uncoated nanofibers were evaluated using a tensile testing machine (Instron Universal Testing Systems 5948). To measure the mechanical properties, nanofiber membranes were cut with dimensions of 23.5 mm length by 10 mm width. The elongation test rate was 5 mm/min. Ultimate tensile stress (MPa) and tensile strain (%) values were measured in triplicate samples.

2.9. Bioadhesion studies

Bioadhesion of a transdermal formulation is required in order to transfer the drug to the skin surface. To determine the bioadhesive performance of transdermal patches on skin, work of bioadhesion values were obtained using a texture analyzer (TA.XT.plus Texture Analyzer, Stable Micro Systems, UK). The outer part of rat skin was shaved and used in bioadhesion studies. The transdermal patches were attached with double-sided tape to the lower end of the probe. The probe was placed in contact with the skin for 120 s. The adhesion was tested with an applied force of 0.2 N and a pulling rate of 1 mm/s. The area under the force – distance (N \times mm) curve was calculated using the software of the instrument and the work of bioadhesion was measured. The measurements were performed in triplicate.

2.10. In-vitro drug release and diffusion studies

To investigate the effect of Parylene coating, drug release studies were performed for 30 days in pH 5.5 phosphate buffer at 32°C , simulating conditions on the skin surface. Optical absorption spectra were taken at predetermined time intervals and the amount of PPX was measured spectrophotometrically at 264 nm using a micro volume spectrophotometer (Nanodrop One, Thermo Fisher Scientific). *In vitro* release data were analyzed to fit to certain kinetic models, such as first order, Higuchi, and Korsmeyer-Peppas, using the DDSolver add-in program with the following equations:

$$\text{First order} : \ln(100 - Q) = \ln 100 - kt \quad (3)$$

$$\text{Higuchi's equation} : Q = k_H t^{1/2} \quad (4)$$

$$\text{Korsmeyer - Peppas} : M_t/M_\infty = k_{KP} t^n \quad (5)$$

where Q is the amount of drug release in time t per unit area, k is the 1st order rate constant, k_H is the Higuchi dissolution constant, M_t/M_∞ is the fraction of drug released at time t , and n is the release exponent.

In vitro diffusion studies were carried out using all-glass Franz diffusion cells in pH 7.4 phosphate buffer at 37°C with cellulose membrane to simulate the epithelium layer of the skin. Nanofiber membrane samples were placed in the donor phase of Franz diffusion cells to which 0.5 ml buffer was dispensed to simulate hydration. At predetermined timepoints, sample solutions were taken from the receptor phase and replenished with fresh buffer solution. The amount of PPX in the sample solution was measured spectrophotometrically.

3. Results and discussion

3.1. Rheological studies

Viscosity is a critical parameter for the electrospinning process. Viscosity that is too low or too high causes problems during electrospinning, such as beaded fibers, electrospayed particles, or limited whipping action. The use of pure PCL with molecular weight of 80 kDa at a concentration of $>10\%$ provides sufficient elasticity of solution for electrospinnability [20]. Both PCL and PPX loaded PCL solutions showed lower viscosity as shear rate increases (Fig. S1). Addition of PPX to the PCL polymer solution decreased the viscosity due to the hydrochloride salt groups of PPX. The viscosity of PCL-PPX solution was sufficient for the electrospinning process [21].

3.2. Fiber morphologies

Electrospinning of PCL solutions with GAA:FA solvent mixture (3:1) resulted in a continuous process with no clogging at the nozzle tip. The acetic acid - formic acid mixture is considered a benign (non-toxic) solvent. The addition of formic acid to acetic acid decreased the nanofiber diameter, due to its higher dielectric constant compared to that of acetic acid [22]. PPX-loaded PCL nanofibers have a fairly uniform diameter and form a bead-less morphology (Fig. 1a). The thickness of Parylene coating is directly related to the amount of starting dimer material used. Coating of Parylene at low amounts (50 mg) affected the nanofiber diameter slightly from 132 ± 25 nm for uncoated fibers (PCL) to 147 ± 34 nm for PPN50 (Fig. 1c) and 156 ± 27 nm for PPC50 (Fig. 1b) ($p > 0.05$). In contrast, high Parylene starting amount (300 mg) increased the nanofiber diameter significantly ($p < 0.05$) (Table 3). This increment was significant especially for Parylene C (Fig. 1d), with the average fiber diameter increasing from ~ 132 to ~ 466 nm. Our results are similar to those of Zeng et al. [23], who reported that 100 mg of parylene dimer resulted in a coating thickness of ~ 100 nm on nanofibers, while 500 mg parylene dimer resulted in a coating thickness on the nanofibers of ~ 300 nm.

3.3. DSC studies

DSC scans were performed to determine if there is an interaction between PPX, PCL host polymer and Parylene coatings. Both Parylene C and N did not exhibit DSC peak up to 200°C . PCL has an endothermic peak at $\sim 60^\circ\text{C}$ due to its melting point. This peak was observed in all nanofiber thermograms (Fig. 2) as expected. The endothermic peak of pure PCL pellets slightly shifted from 59 to 62°C . Similar peak shifts were reported for PCL nanofibers. Solvent evaporation during electrospinning process affected the rearrangement and crystallization

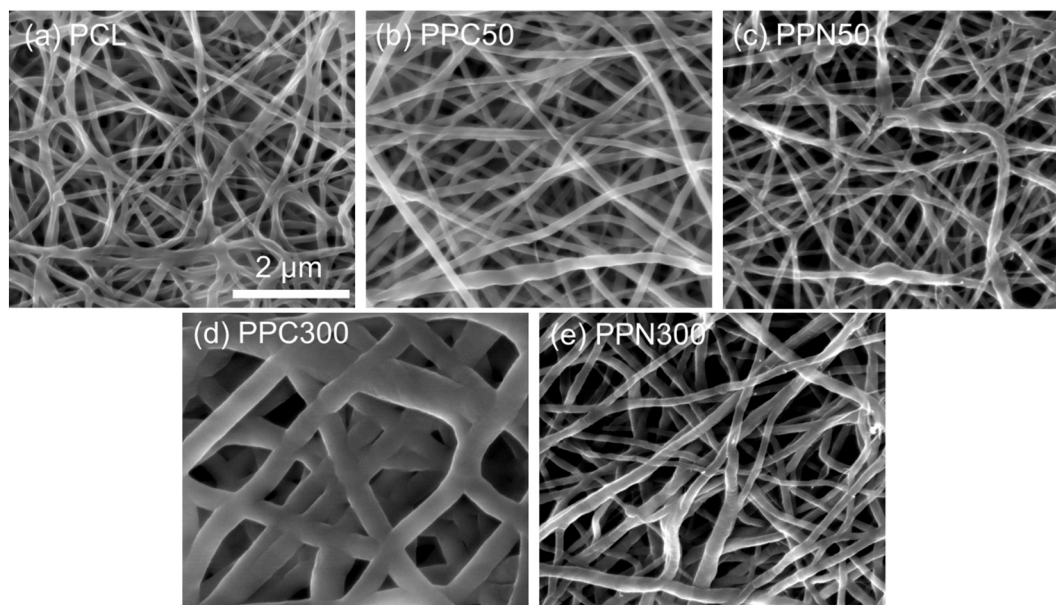


Fig. 1. SEM images of fiber membranes formed by several formulations: (a) PCL; (b) Parylene C, 50 mg (PPC50); (c) Parylene N, 50 mg (PPN50); (d) Parylene C, 300 mg (PPC300); (e) Parylene N, 300 mg (PPN300).

Table 3
Different characterization results of uncoated and parylene-coated formulations.

Formulation code	Mean diameter (nm)	Work of bioadhesion (mJ/m ²)	Porosity (%)	Water contact angle (°)	Tensile test			Franz diffusion test	
					UTS (MPa)	Strain (%)	Young's modulus (MPa)	Flux (μg/cm ² /h)	Permeability coefficient (cm/h)
PCL	132 ± 25	115.9	80.3	112.5 ± 1.1	1.3 ± 0.1	28.4 ± 1.8	4.9 ± 0.2	285.7 ± 75.4	0.336 ± 0.09
PPC50	156 ± 27	60.1	86.5	123.6 ± 0.9	2.3 ± 0.2	28.5 ± 2.3	10.0 ± 0.9	25.2 ± 12.6	0.008 ± 0.004
PPN50	147 ± 34	213.2	80.6	124.8 ± 9.7	1.6 ± 0.2	25.8 ± 3.7	7.3 ± 0.3	36.6 ± 2.4	0.036 ± 0.002
PPC300	466 ± 91	31.3	86.0	134.3 ± 3.2	5.1 ± 0.1	69.8 ± 8.2	67.1 ± 7.2	–	–
PPN300	218 ± 50	111.8	80.0	129.4 ± 3.0	1.4 ± 0.2	24.0 ± 3.5	9.7 ± 2.6	–	–

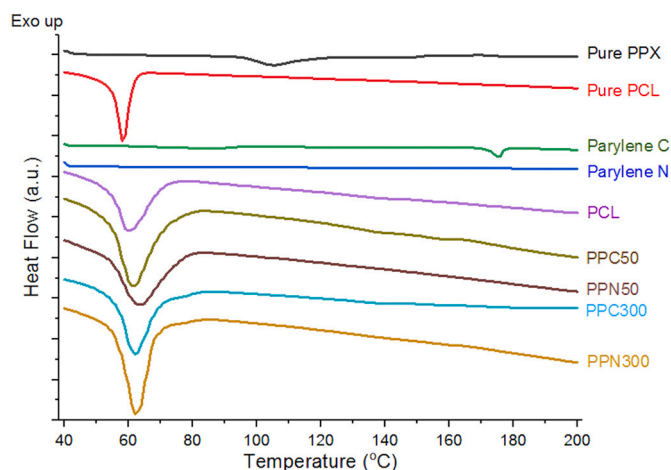


Fig. 2. DSC thermograms of PCL polymer, PPX and nanofiber formulations.

behavior of PCL polymer chains [24]. PPX has crystalline water in its structure, which causes a broad endothermic peak at ~100–140 °C. This endothermic peak was not observed in the nanofiber membrane

thermograms, possibly because the electrospinning process causes the conversion of PPX from crystalline to amorphous structure. Another possibility is that since PCL has a very low melting point compared to PPX the latter can dissolve in melted PCL, hence the absence of its endothermic peak in the nanofiber formulations [25]. Clearly, incorporated PPX is well dissolved into the host PCL nanofiber materials for all cases.

3.4. NMR and XRD studies

In Fig. 3, NMR results showed the confirmation of the presence of the PPX in the PCL nanofibers. The peaks at ~9.5 ppm corresponding to the –NH₂ protons and ~0.9 ppm corresponding to the –CH₃ protons are due to PPX. The more significant PPX peak at 0.9 ppm is evident in all nanofiber NMR spectra, with intensity dependent on the ratio of PPX drug to polymer.

In XRD spectra (Fig. 4), pure PPX exhibited characteristic peaks at 21.34° and 24.76° indicating the crystalline form of the drug and pure PCL exhibited two characteristic peaks at 22.66° and 25.06° due to the (110) and (200) reflections [26]. While all nanofiber formulations showed the characteristic peaks of PCL, no characteristic peaks of PPX were detected in nanofiber formulations indicating a transformation of PPX state from crystalline to amorphous form in nanofibers. The loss of

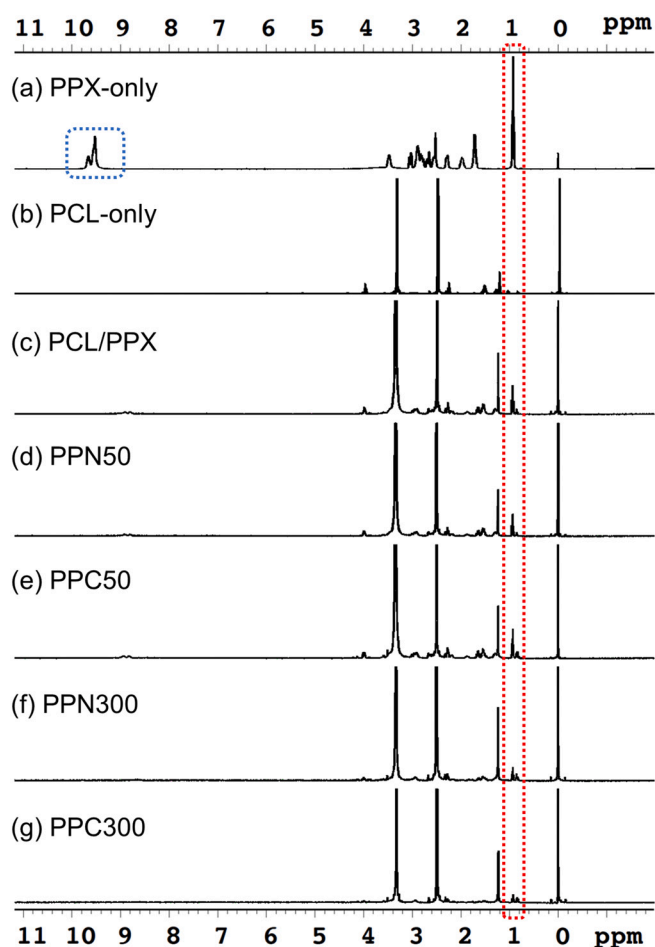


Fig. 3. NMR results for (a) pure PPX powder; (b) PCL pellets; (c) PCL nanofibers; (d) PPN50 nanofibers; (e) PPC50 nanofibers; (f) PPN300 nanofibers; (g) PPC300 nanofibers. All nanofiber formulations include a PPX drug.

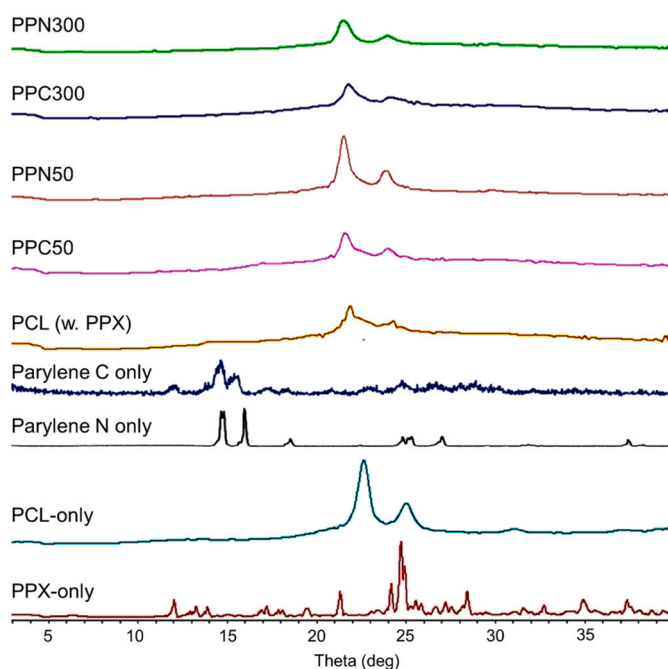


Fig. 4. XRD diffractograms of PCL, PPX, Parylenes and their nanofiber formulations.

crystallinity was consistent with the DSC results.

3.5. Wettability, porosity, bioadhesion and mechanical properties of nanofibers

Fig. 5 shows the effect of Parylene coating on the wettability and bioadhesion of the resulting fiber membranes. PCL is a hydrophobic polymer and its nanofiber membrane form showed a water contact angle (WCA) of $\sim 125\text{--}130^\circ$ [27,28]. The loading of hydrophilic drug PPX decreased the contact angle. In our study, the WCA of PPX-containing PCL fiber membranes was found to be $\sim 112^\circ$, as shown in Fig. 5a. The addition of hydrophilic materials has been reported to decrease WCA. For example incorporating gelatin into PCL fibers results in a WCA change from 130° for PCL fibers to 37° for PCL/gelatin blended fibers [29]. In addition, the WCA of PCL cast film was found to be 93° , which indicates a smoother surface compared to nanofibers. Gharaei et al. reported that porous microstructure plays a significant role on wettability [30]. On the other hand, coating with Parylene (that has hydrophobic characteristics) has resulted in an overall increase in WCA (Fig. 5a). The use of 50 mg Parylene C and N increased the WCA by $\sim 10^\circ$, while the use of 300 mg Parylene C and N increased the WCA by 22° and 17° , respectively. Parylene C is known to have superior water and gas barrier properties compared to Parylene N [17]. WCAs of Parylene N, C and D have been reported as 79° , 87° and 97° , respectively [31]. Parylene C coated micro-structured surfaces have been reported to have a WCA of $\sim 130^\circ$, while flat homogeneous Parylene films have a contact angle of $\sim 90^\circ$ [32]. Our porous nanofiber surfaces provide micro-roughness on the surface, leading to the increased water contact angle compared to homogenous Parylene films [33].

Membrane porosity values of certain nanofiber formulations were affected by Parylene coating. Parylene N coating did not affect the porosity values, whereas Parylene C coating increased slightly the porosity values of PPC50 and PPC300 formulations from 80.3% to 86.5% and 86.0%, respectively. While the increased porosity does not present the significant effect on the hydrophobicity of membranes, the hydrophobic nature of Parylene coating diminishes the effect of hydrophilic PPX addition, leading to the increased hydrophobicity of Parylene coated membranes.

As expected, higher hydrophobicity (lower wettability) of Parylene coated membranes generally resulted in lower bioadhesion (Fig. 5b). Although some studies used PCL nanofibers for transdermal delivery of drugs [4,34], bioadhesion of the Parylene coated PCL membranes can be improved by adding an adhesive backing layer.

The mechanical properties (ultimate tensile stress (UTS), strain at breakdown, and Young's modulus) of Parylene-coated PCL fiber membranes were investigated as shown in Fig. 6. Parylene C has higher tensile strength (Fig. 6a) and elongation at break (Fig. 6b) values compared to Parylene N. At lower Parylene coating amounts (50 mg), tensile stress and strain values did not change significantly compared to non-coated PCL nanofibers due to the thin coating thickness. The highest tensile stress and strain values were achieved with the higher amount (300 mg) of Parylene C coating. Similarly, Cieslik et al. reported that, for Parylene C coatings the critical load for initial cracks is $\sim 5\times$ higher than Parylene N [35]. They also reported that Parylene N coatings are tough and brittle because of higher crystallinity, while Parylene C exhibits higher elasticity. The ultimate tensile stress and tensile strain values were suitable for use the formulations as a transdermal patch on the skin [36].

3.6. Drug release and diffusion studies

Sustained release of hydrophilic drugs, such as PPX, is problematic compared to hydrophobic drugs. Eskitoros-Togay et al. prepared PCL nanofibers containing hydrophilic doxycycline drug, with a drug to polymer ratio of 3.5:12 and reported that the entire drug content was released within 8 h [37]. In our study, PCL formulation without Parylene

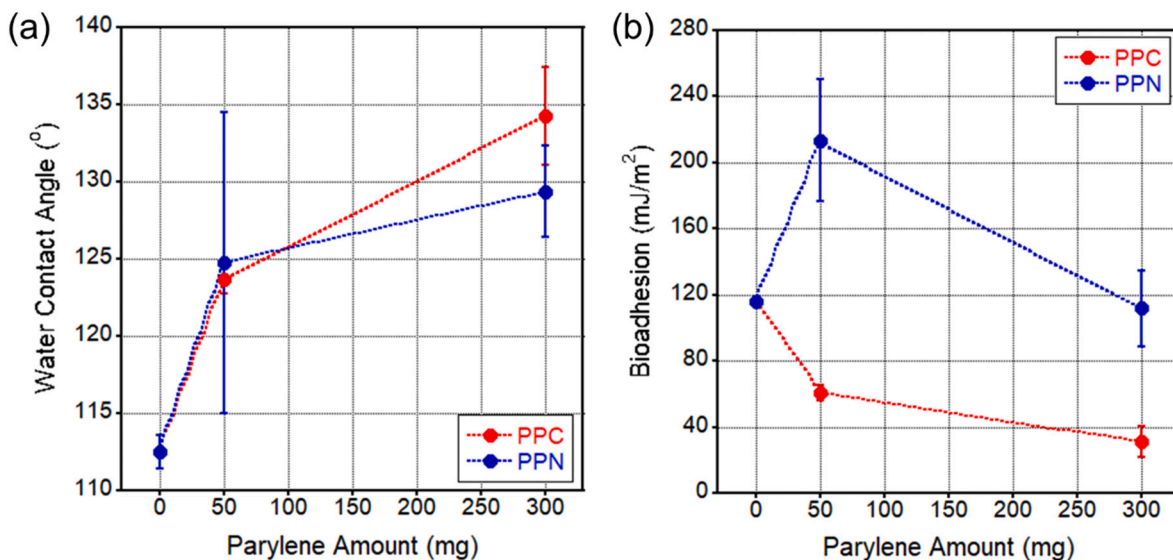


Fig. 5. Effect of Parylene amounts for CVD processes on (a) water contact angles and (b) bioadhesion energy of different formulations ($n = 3$).

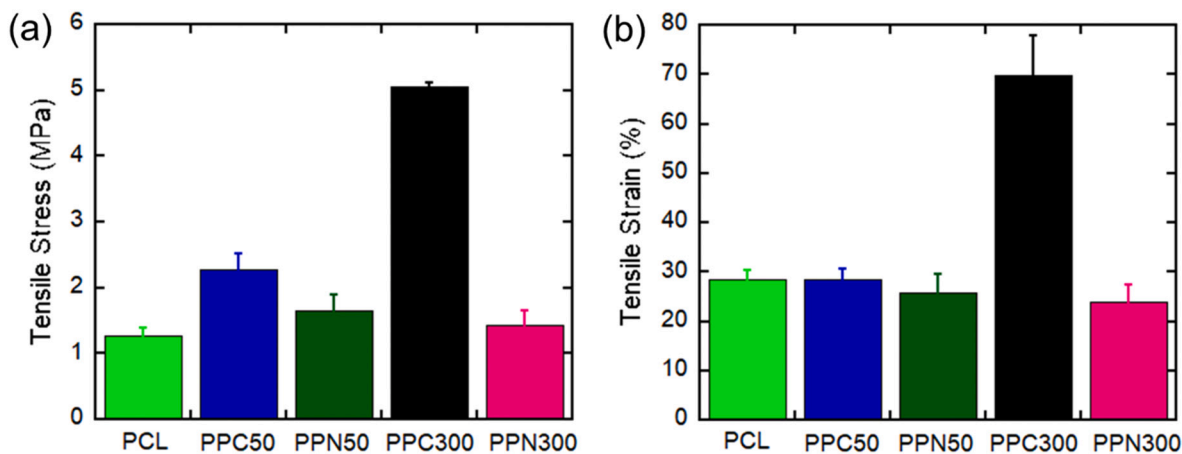


Fig. 6. Mechanical properties of different formulations: (a) ultimate tensile strength; (b) tensile strain.

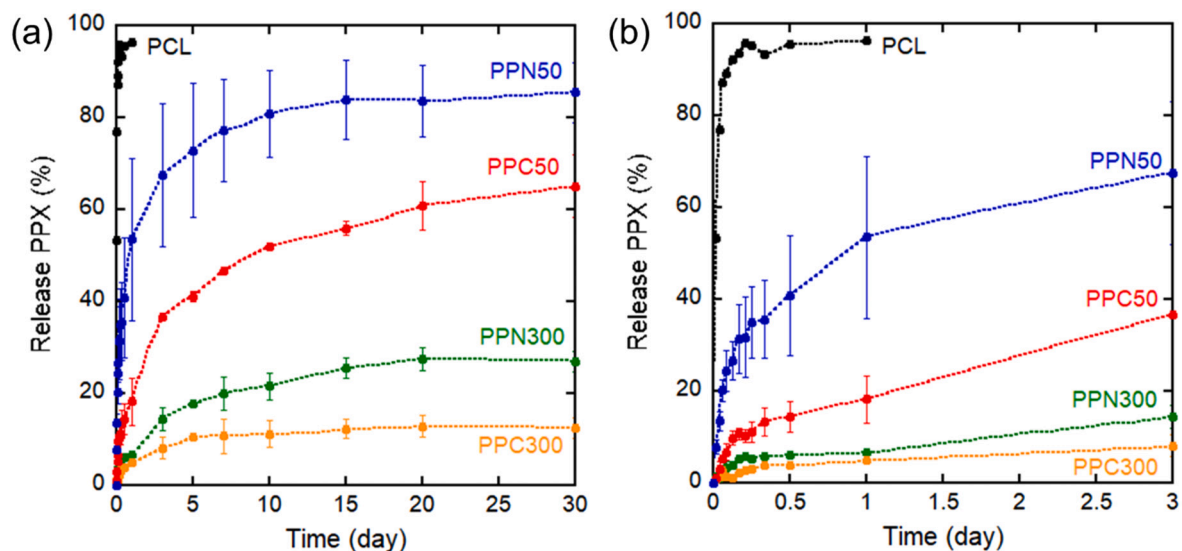


Fig. 7. PPX release profiles of the various formulations over periods of: (a) 30 days; (b) 3 days.

coating showed a rapid PPX release profile even at drug to polymer ratio of 1:20. The goal of the Parylene coating is to prevent the burst release of the hydrophilic drug by adding a hydrophobic sheath layer. The advantage of Parylene vapor deposition is producing a conformal coating that is imperforated over the entire surface. This has successfully prevented the burst release of the drug from the fiber surfaces (Fig. 7). While PCL-only nanofiber membranes entirely released their PPX content in ~12 h, membranes coated with Parylene provided an excellent barrier extending the PPX release significantly. In particular, the membranes coated with 300 mg of Parylene displayed continued slow release over a period of several weeks, consistent with their decreased wettability and thicker effective fiber diameter. Over a period of 30 days, the PPC300 and PPN300 formulations released ~10% and ~20% drug, respectively. Drug release from the thicker Parylene coating occurred very slowly. Parylene C decreased the drug release significantly more than Parylene N due to its chemical structure (a chlorine atom on the benzene ring) and coating thickness. Although Parylene C and N both have very low water absorption values (<0.1% in 24 h), Parylene C has lower water vapor transmission rate of 0.08 (g·mm)/(m²·day) compared to 0.59 (g·mm)/(m²·day) for Parylene N, which may contribute to the slower drug release [31]. This clearly indicates that increasingly long-term release can be achieved with by increasing the Parylene coating thickness. Similarly, the decreased release of BSA from PVA nanofibers was reported with increased Parylene C coating thickness [23]. The lower amount (50 mg) of Parylene coating also resulted in the prevention of PPX burst release, albeit at a faster rate than the thicker coating. PPC50 formulation released ~60% drug in 30 days, while PPN50 formulation released ~80% drug in 30 days. The lower amount of Parylene provided faster release profiles and is more practical for transdermal drug delivery. As seen in Table 4, while the release kinetics showed a good fit to the First order model without Parylene coating, all data showed good fit in the Korsmeier-Peppas model ($r^2 = 0.908$ to 0.962) after Parylene coating. The release exponent values were found to be between 0.173 and 0.465, which indicates pseudo-Fickian (partial diffusion) ($n < 0.5$) diffusion mechanism. As expected, based on n values of <0.5, the release from non-degradable Parylene occurs primarily by diffusion rather than by erosion.

Long term exposure to transdermal patches (more than a month) could result in skin irritation. Therefore, *in vitro* drug diffusion studies were carried out with PPN50 and PPC50 formulations. Franz diffusion experiments were used to evaluate the *in vitro* drug permeation for the prediction of the performance of transdermal administration. Similar to the drug release study, PPX in uncoated PCL fibers permeated rapidly compared to PPN50 and PPC50 formulations at pH of 7.4 (Fig. 8). The flux value of uncoated PCL decreased ~10× compared to Parylene-coated formulations through dialysis membrane (Table 3). Fast release of PPX from uncoated PCL nanofibers resulted in high concentration gradient and provided rapid permeation through the skin-mimicking cellulose membrane between donor and receptor phases. Parylene coating created a barrier outside of nanofibers and decreased the released drug. With this reduction, both flux and permeability coefficient values decreased accordingly. The similarity between drug release and diffusion profiles indicates that released drugs are easily diffused through the membrane because of the small molecular weight of PPX (~302.3 Da).

4. Conclusion

Nanofibers represent a new platform for drug delivery systems in the pharmaceutical world due to their unique properties. In this study, PPX-loaded nanofibers were successfully coated with different Parylene types and amounts using chemical vapor deposition method. The initial burst release of PPX from PCL nanofibers was successfully prevented with parylene coating, enabling long-term release kinetics. Pinhole-free conformal coating enables the sustained release from the hydrophilic drug incorporated nanofiber patches. Parylene C coating layer provided

Table 4
Kinetics of drug release from nanofiber formulations.

	First order		Higuchi		Korsmeier-Peppas		
	r^2	k	r^2	k_H	r^2	n	k_{KP}
PCL	0.982	1.51	0.799	57.9	0.967	0.259	71.3
PPC50	0.771	0.0669	0.929	14.14	0.908	0.465	17.75
PPN50	0.331	0.134	0.466	21.29	0.925	0.173	47.98
PPC300	0.429	0.00679	0.848	3.13	0.937	0.374	4.68
PPN300	0.657	0.0148	0.934	6.18	0.962	0.436	7.17

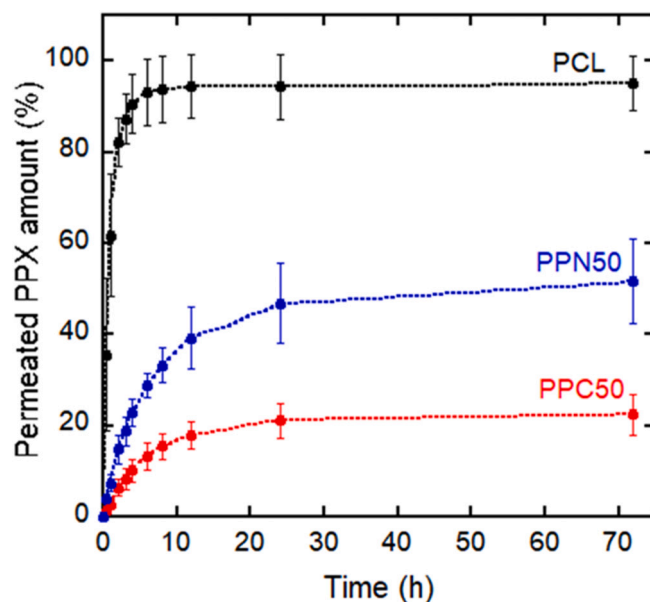


Fig. 8. PPX diffusion profiles measured from Franz diffusion cell up to 72 h.

more retarded release kinetics compared to that of Parylene N. This study demonstrated a versatile approach that combines the prevention of burst release of a hydrophilic drug with the ability to adjust release profiles with coating thickness, thus providing a suitable release profile for long term transdermal drug delivery as well as wound dressing and drug loaded stent applications.

Supplementary data to this article can be found online at <https://doi.org/10.1016/j.surfcoat.2021.126831>.

CRedit authorship contribution statement

Serdar Tort: Conceptualization, Methodology, Experiments, Characterization, Writing. **Daewoo Han:** Characterization, Analysis, Writing. **Eric Frantz:** Software. **Andrew Steckl:** Writing, Reviewing and Editing.

Declaration of competing interest

The authors declare that they have no known competing financial interests or personal relationships that could have appeared to influence the work reported in this paper.

Acknowledgements

ST was awarded a scholarship by the Scientific and Technical Research Council of Turkey [TUBITAK-BIDEB 2219].

References

- [1] R.J. Markovich, A.K. Taylor, J. Rosen, J. Pharm. Biomed. Anal. 16 (1997) 651–660.

- [2] T.E.G.K. Murthy, V. Kishore, *Indian J. Pharm. Sci.* 69 (2007) 646–650.
- [3] P.R. Rao, P.V. Diwan, *Pharm. Acta Helv.* 72 (1997) 47–51.
- [4] K. Madhaiyan, R. Sridhar, S. Sundarajan, J.R. Venugopal, S. Ramakrishna, *Int. J. Pharm.* 444 (2013) 70–76.
- [5] J. Xue, T. Wu, Y. Dai, Y. Xia, *Chem. Rev.* 119 (2019) 5298–5415.
- [6] D. Han, S. Sherman, S. Filocamo, A.J. Steckl, *Acta Biomater.* 53 (2017) 242–249.
- [7] Y. Ding, W. Li, F. Zhang, Z. Liu, N. Zanjanzadeh Ezazi, D. Liu, H.A. Santos, *Adv. Funct. Mater.* 29 (2019) 1802852.
- [8] D. Han, A.J. Steckl, *ACS Appl. Mater. Interfaces* 5 (2013) 8241–8245.
- [9] X. Li, Y. Gong, *J. Chem.* 2015 (2015) 460392.
- [10] K. Ghosal, A. Chandra, G. Praveen, S. Snigdha, S. Roy, C. Agatemor, S. Thomas, I. Provaznik, *Sci. Rep.* 8 (2018) 5058.
- [11] Y. Wang, X. Yu, P. Zhang, Y. Ma, L. Wang, H. Xu, D. Sui, *J. Pharmacol. Sci.* 138 (2018) 31–37.
- [12] Y. Li, D. Wang, S. Lu, L. Zeng, Y. Wang, W. Song, J. Liu, *Eur. J. Pharm. Sci.* 124 (2018) 80–88.
- [13] M.A. Surmeneva, A. Vladescu, C.M. Cotrut, A.I. Tyurin, T.S. Pirozhkova, I. A. Shuvarin, B. Elkin, C. Oehr, R.A. Surmenev, *Appl. Surf. Sci.* 427 (2018) 617–627.
- [14] E. Robinson, S. Kaushal, J. Alaboson, S. Sharma, A. Belagodu, C. Watkins, B. Walker, G. Webster, P. McCarthy, D. Ho, *Nanoscale* 8 (2016) 4267–4275.
- [15] E. Pierstorff, R. Lam, D. Ho, *Nanotechnology* 19 (2008) 445104.
- [16] M. Chen, H. Huang, E. Pierstorff, E. Shin, E. Robinson, D. Ho, *Ann. Biomed. Eng.* 37 (2009) 2003–2017.
- [17] M. Golda-Cepa, K. Engvall, M. Hakkarainen, A. Kotarba, *Prog. Org. Coat.* 140 (2020) 105493.
- [18] D.X. Oh, *Mater. Sci. Forum* 926 (2018) 73–78.
- [19] D. Han, S.T. Boyce, A.J. Steckl, *MRS Proceedings* 1094 (2008), 1094-DD1006-1002.
- [20] A. Cipitria, A. Skelton, T.R. Dargaville, P.D. Dalton, D.W. Huttmacher, *J. Mater. Chem.* 21 (2011) 9419–9453.
- [21] Y.-F. Li, M. Rubert, H. Aslan, Y. Yu, K.A. Howard, M. Dong, F. Besenbacher, M. Chen, *Nanoscale* 6 (2014) 3392–3402.
- [22] S. Bongiovanni Abel, L. Liverani, A.R. Boccaccini, G.A. Abraham, *Mater. Lett.* 245 (2019) 86–89.
- [23] J. Zeng, A. Aigner, F. Czubyko, T. Kissel, J.H. Wendorff, A. Greiner, *Biomacromolecules* 6 (2005) 1484–1488.
- [24] X. Wang, H. Zhao, L.-S. Turng, Q. Li, *Ind. Eng. Chem. Res.* 52 (2013) 4939–4949.
- [25] T. Potrc, S. Baumgartner, R. Roskar, O. Planinsek, Z. Lavric, J. Kristl, P. Kocbek, *Eur. J. Pharm. Sci.* 75 (2015) 101–113.
- [26] J.S. Lyu, J.-S. Lee, J. Han, *Sci. Rep.* 9 (2019) 20236.
- [27] A. Martins, E.D. Pinho, S. Faria, I. Pashkuleva, A.P. Marques, R.L. Reis, N.M. Neves, *Small* 5 (2009) 1195–1206.
- [28] D. Han, A.J. Steckl, *Langmuir* 25 (2009) 9454–9462.
- [29] I. Unalan, S.J. Endlein, B. Slavik, A. Buettner, W.H. Goldmann, R. Detsch, A. R. Boccaccini, *Pharmaceutics* 11 (2019) 570.
- [30] R. Gharaei, G. Tronci, R.P.W. Davies, C. Gough, R. Alazragi, P. Goswami, S. J. Russell, *J. Mater. Chem. B* 4 (2016) 5475–5485.
- [31] C.P. Tan, H.G. Craighead, *Materials* 3 (2010) 1803–1832.
- [32] Z. Wang, L. Xu, X. Wu, J. Chen, *Microsyst. Nanoeng.* 4 (2018) 17099.
- [33] J. Jaiswal, A. Sanger, A. Kumar, S. Mourya, S. Chauhan, R. Daipuriya, M. Singh, R. Chandra, *Adv. Mater. Lett.* 7 (2016) 485–490.
- [34] R. Ravikumar, M. Ganesh, V. Senthil, Y.V. Ramesh, S.L. Jakki, E.Y. Choi, *J. Drug Deliv. Sci. Tec.* 44 (2018) 342–348.
- [35] M. Ciešlik, M. Kot, W. Reczyński, K. Engvall, W. Rakowski, A. Kotarba, *Mater. Sci. Eng. C* 21 (2012) 31–35.
- [36] G. Jin, Y. Li, M.P. Prabhakaran, W. Tian, S. Ramakrishna, *J. Bioact. Compat. Polym.* 29 (2014) 628–645.
- [37] Ş.M. Eskitoros-Togay, Y.E. Bulbul, S. Tort, F. Demirtaş Korkmaz, F. Acartürk, N. Dilsiz, *Int. J. Pharm.* 565 (2019) 83–94.
- [38] Parylene barrier properties: why aren't all my electronics waterproof?. <http://vsiparylene.com/2017/2012/2012/parylene-electronics-waterproof/>.

Controlled Drug Release of Parylene-Coated Pramipexole Nanofibers for Transdermal Applications

Serdar Tort^{a,b}, Daewoo Han^a, Eric Frantz^a, Andrew J. Steckl^{a,*}

^aNanoelectronics Laboratory, Electrical Engineering and Computer Science, University of Cincinnati, Cincinnati 45221-0030, USA

^bDepartment of Pharmaceutical Technology, Faculty of Pharmacy, Gazi University, Ankara 06330, Turkey

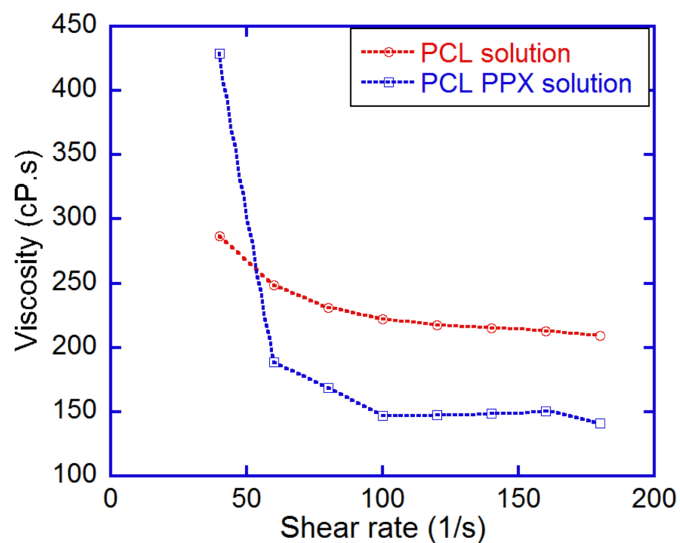


Figure S1 Rheological properties of PCL and PCL/PPX polymer solutions.